AIP | Journal of Applied Physics

Theory of photoemission from cesium antimonide using an alpha-semiconductor model

Kevin L. Jensen, Barbara L. Jensen, Eric J. Montgomery, Donald W. Feldman, Patrick G. O'Shea, and Nathan Moody

Citation: Journal of Applied Physics **104**, 044907 (2008); doi: 10.1063/1.2967826
View online: http://dx.doi.org/10.1063/1.2967826
View Table of Contents: http://scitation.aip.org/content/aip/journal/jap/104/4?ver=pdfcov
Published by the AIP Publishing

Theory of photoemission from cesium antimonide using an alpha-semiconductor model

Kevin L. Jensen,[1,a)] Barbara L. Jensen,[2,b)] Eric J. Montgomery,[2] Donald W. Feldman,[2] Patrick G. O'Shea,[2] and Nathan Moody[3]
[1]*Code 6843, ESTD, Naval Research Laboratory, Washington, DC 20375-5347, USA*
[2]*Institute for Research in Electronics and Applied Physics, University of Maryland, College Park, Maryland 20742-3511, USA*
[3]*Los Alamos National Laboratory, Los Alamos, New Mexico 87545-1362, USA*

(Received 29 April 2008; accepted 8 June 2008; published online 28 August 2008)

A model of photoemission from cesium antimonide (Cs_3Sb) that does not rely on adjustable parameters is proposed and compared to the experimental data of Spicer [Phys. Rev. **112**, 114 (1958)] and Taft and Philipp [Phys. Rev. **115**, 1583 (1959)]. It relies on the following components for the evaluation of all relevant parameters: (i) a multidimensional evaluation of the escape probability from a step-function surface barrier, (ii) scattering rates determined using a recently developed alpha-semiconductor model, and (iii) evaluation of the complex refractive index using a harmonic oscillator model for the evaluation of reflectivity and extinction coefficient. © *2008 American Institute of Physics*. [DOI: 10.1063/1.2967826]

INTRODUCTION

Cesium-based photocathodes using a dispenser architecture are sought for high average power free electron lasers (FELs)[1–3] as they exhibit good quantum efficiency (QE) at wavelengths that should not unduly burden existing drive lasers for pulse durations and repetitions characteristic of high average current. Photocathodes may represent the only electron source able to meet the performance requirements (in terms of current and emittance) of FELs; yet, modern accelerator environments[4,5] are known to be damaging to the cesiated surfaces of high QE photocathodes. Thus, the dispenser architecture[6] is under investigation to determine how well the surface can be rejuvenated after degradation.[5,7–9] As part of the program to develop a controlled porosity dispenser photocathode, a predictive theoretical model of photoelectron emission from the surface is required. In addition, the theoretical photoemission model (as was true with its metal and coated metal predecessors[8,10]) must be amenable to incorporation into advanced beam simulation codes that model vacuum electronic devices and the dynamic evolution of bunched electron beams,[11–13] and such requirements make constraints on the complexity of the numerical evaluations implicit in the application of the emission model. This work will describe the development of the emission theory and its numerical realization.

The proposed theory is to be contrasted with Spicer's three-step model,[14–16] which is a widely used description of photoemission used to characterize both semiconductors[17,18] and metals[19] (see, also, the theory developed by Kane[20]) The alkali-antimonide surfaces are semiconductors exhibiting high QE[14,21,22]) and have been characterized using the Spicer model, in which parameters associated with the escape probability and the absorption coefficient are adjusted to conform with experimental data. In contrast, the model to be developed here differs in regard to its effort to eliminate adjustable parameters by relying on physical models of the underlying processes. Its foundation, as well as its success in predicting the QE from bare and coated metals[8,10] and photoemission emittance,[23] has been treated elsewhere. In contrast to metals, semiconductors exhibit additional complexity, such as band bending, the inclusion of phonon and impurity scattering mechanisms,[24,25] electron effective mass, and other difficulties. The present work therefore seeks to account for some of these issues by augmenting the framework of the model previously developed for cesiated surfaces but again with the intent of minimizing a reliance on parameters deduced from fits to data; other issues, such as band bending due to high field, are not presently treated in the weak field limit we consider.

There are three processes to be addressed. First, the escape probability for low electron affinity surfaces is not a step function in energy as frequently assumed. Second, the energy-dependent scattering rates figuring prominently in the function governing electron transport to the surface require specification. Finally, the reflectivity and laser penetration depth determined from the complex refractive index are the last factors influencing the quantum yield. In what follows, each of these processes will be accounted for using fundamental models of the underlying processes to reduce the dependence of the theoretical predictions on *ad hoc* parameters and allow the model to be predictive. The formulation is applied to the special case of cesium antimonide (Cs_3Sb) because of its centrality in our investigation to determine if depleted cesium can be rejuvenated by a dispensation of additional cesium analogous to the process utilized by conventional dispenser cathodes.[1,5,9] In a separate work, the impact of a finite layer thickness instead of the bulk (infinite thickness) conditions treated here shall be considered.

[a)]Electronic mail: kevin.jensen@nrl.navy.mil.
[b)]Retired.

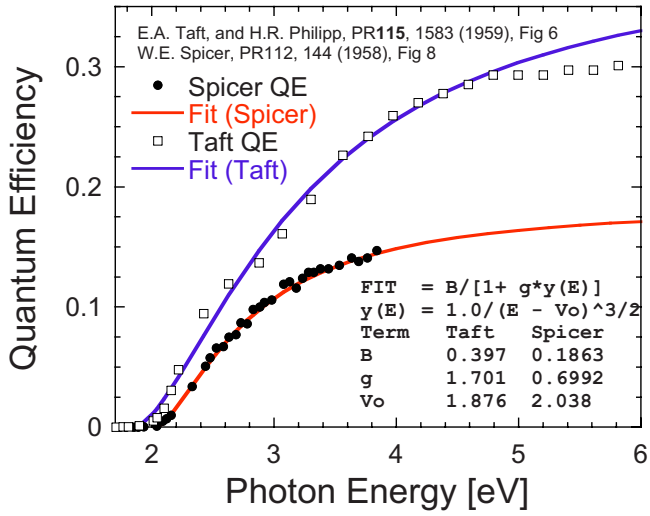

FIG. 1. (Color online) The experimental yield (QE) data of Spicer (solid circle) and Taft and Philipp (open square) compared to a least-squares fit: Least-squares values differ slightly from those reported by Spicer and Taft and Philipp.

REVIEW OF EXPERIMENTAL DATA USING THE SPICER THREE-STEP MODEL

The experimental data for the quantum yield of Cs_3Sb obtained by both Spicer[14] and separately by Taft and Philipp[26] are shown in Fig. 1 alongside fits based on the three-step model [Eq. (6) of Ref. 14] parametrically represented as

$$\mathrm{QE} \approx \frac{B}{1+g(E-V_0)^{-p}}, \tag{1}$$

where B and g are constant and $V_0=E_g+E_a$, where E_g is the band gap and E_a is the electron affinity. The simple form of Eq. (1) is based on the presumption that the probability of emission (in Spicer's notation) is given by

$$P(x,\hbar\omega) = G(\hbar\omega)e^{-\beta x} \approx Be^{-\beta x}, \tag{2}$$

where x is the depth into the crystal from the surface, β is the inverse escape depth,[16] and the function G as shall be seen below owes its origins to the quantum mechanical transmission probability of photoexcited electrons. The power p on $(E-V_0)$ is an empirically determined relation found to be $p=3/2$ (though Eckart[27] gave a value of $p=1.4$ from PbS studies) in separate studies. Equation (1) is a successful semiempirical approach, and the methodology and theory from which it is obtained is widely used (e.g., Refs. 19 and 28–32).

The least-squares extraction of the B, g, and V_0 parameters are given in Table I and show small departures from the values given by Spicer or Taft and Philipp. In Table I, the value of p was not varied from 1.5 (we note in passing that for Spicer's data, the least-squares values if p is allowed to vary are $B=0.176$, $g=0.604$, $p=1.72$, and $V_0=2.00$). Some difference with the values found by Spicer may be due to the neglect of experimental data above 4 eV, where electron scattering with valence electrons reduces the QE,[21] and others due to the methods used to find the least-squares estimates of the parameters, but the differences are not significant. Given that the accepted value of the band gap for Cs_3Sb is $E_g=1.6$ eV, the estimate of electron affinity E_a using Eq. (1) and Table I is here found to be 0.438 eV for Spicer's data (compare to Spicer's finding of 0.45 eV) and 0.276 eV for Taft and Philipp's data (compare to their finding of 0.4 ± 1 eV). The differences between Taft and Philipp's values of B and g compared to Spicer's are more striking (though the ratio B/g, interpreted as the slope of QE with respect to energy when the photon energy is at threshold, is similar) and does not have a ready explanation as long as the photoemission theory relies on fitted parameters. The electron affinity E_a, though an "input" parameter, is subject to variation due to possible differences in composition.[33] Estimates of E_a are made based on the assumption that the quantum mechanical transmission probability for the electron affinity barrier is a step function in energy (the approximation used in the derivation of the Richardson equation for thermionic emission[34]). When that approximation is not used (see, for example, Ref. 28), as shown below, the estimates E_a based on QE measurements are smaller. We now turn to a theoretical analysis that provides a photoemission model not dependent on fitted parameters but rather on models of the underlying phenomena.

THE PHOTOEMISSION MODEL

The evaluation of QE for p-type semiconductors such as Cs_3Sb shall be estimated using a ratio of moments terms as done in Eq. (43) of Ref. 10, except that the initial absence of electrons in the conduction band for a p-type semiconductor modifies the distribution functions for the electrons. As deduced from Eq. (43) in Ref. 10, the current density for the photoexcited electrons is given by

$$J_\lambda = \frac{2qm}{\pi^2\hbar^3}[1-R(\omega)]I_0 \times \int_{E_a}^{\hbar\omega-E_g} E\left[\int_{\varphi(E)}^{1} xf_\lambda(x,E)D(Ex^2)dx\right]dE, \tag{3}$$

where E is the total energy of the photoexcited electron measured with respect to the bottom of the conduction band; $x=\cos(\theta)$ where θ is the polar angle measured with respect to the normal to the surface; $\hbar\omega$, E_g, and E_a are the energy of

TABLE I. Least-squares fits of three-step model Parameters of Eq. (1) to the Cs_3Sb data of Spicer (Ref. 14) and Taft and Philipp (Ref. 26).

Parameter	B	g	p	V_0	B/g
Spicer	0.1863	0.6992	1.5	2.038	0.2664
Taft and Philipp	0.397	1.701	1.5	1.876	0.2334

the incident photon, the band gap, and the electron affinity, respectively; $\varphi(E)=\sqrt{E_a/E}$; q is the elementary charge and m is the effective mass; $R(\omega)$ is the reflectivity of the surface; I_0 is the incident laser intensity; and $D(E)$ is the transmission probability for an electron incident on a barrier of height E_a. Temperature and field dependence are implicit in f_λ and $D(E)$. The scattering factor f_λ accounts for the probability an electron will suffer a collision on its path to the surface, and is given by

$$f_\lambda(x,E)=\frac{x}{x+p(E)},$$
$$p(E)=\frac{m\delta(\hbar\omega)}{\hbar k(E)\tau(E)}, \tag{4}$$

where $p(E)$ is recognized as the ratio between the laser penetration depth δ and the distance an electron travels between collisions, i.e., the product of its velocity and the scattering time. QE is then the ratio of J_λ with the maximum current density, defined by a formula similar to Eq. (3) but in which the transmission probability and scattering factor are unity, and the energy integration lower bound is 0, or

$$J_{\max}=2\frac{2qm}{\pi^2\hbar^3}I_0\int_0^{\hbar\omega-E_g}E\left[\int_0^1 xdx\right]dE=\frac{mq}{\pi^2\hbar^3}\Delta^2 I_0, \tag{5}$$

where $\Delta\equiv\hbar\omega-E_g$ is the difference between the photon energy and the band gap. A coefficient of 2 accounts for electrons being able to travel in any direction, not just the forward direction. QE is then given by the ratio $\mathrm{QE}=J_\lambda/J_{\max}$. The program for its evaluation is to evaluate the transmission probability, relaxation time, laser penetration depth, and reflectivity: Each of these shall be considered based on representative models.

Before proceeding to do so, a convenient approximation, as observed by Fowler,[35] is obtained by replacing $D(Ex^2)$ $\approx D(E)$; it functions reasonably well for metals and is the basis for the Fowler–Dubridge model. Using this approximation for semiconductors gives

$$\mathrm{QE}_0=\frac{1}{2}[1-R(\omega)]\int_{E_a}^{\hbar\omega-E_g}ED(E)F_\lambda\left(\sqrt{\frac{E}{E_a}}\right)dE$$
$$=\frac{1}{2}[1-R(\omega)]G_\lambda\left(\sqrt{\frac{\Delta}{E_a}}\right), \tag{6}$$

where the introduced functions $F_\lambda(y)$ and $G_\lambda(y)$ are defined by

$$F_\lambda(y)=\int_y^1 xf_\lambda(x,E_a y^2)dx$$
$$=\frac{1}{2y^2}(1-y)[2yp(E)-y-1]$$
$$+p(E)^2\ln\left[y\left(\frac{1+p(E)}{1+yp(E)}\right)\right],$$
$$G_\lambda(y)=\frac{8}{y^4}\int_1^y x^3F_\lambda(x)dx. \tag{7}$$

The quantity $\Delta\mathrm{QE}\equiv\mathrm{QE}-\mathrm{QE}_0$ therefore is an indication of the extent to which the one-dimensional approach of Eq. (6) overestimates the QE for semiconductors as calculated using a moments-based approach described in Ref. 10: Given that QE_0 is numerically easier to evaluate than QE, it represents a perhaps more useful first estimate of the QE of Cs_3Sb.

Transmission probability

Triangular-barrier model

The (one-dimensional) transmission probability for a triangular-barrier potential of height E_a and field F, familiar from the Fowler–Nordheim equation of field emission, is given by [from Eq. (10) of Ref. 36—though compare Eq. (23) of Ref. 37]

$$D_\Delta(E)=\frac{4\sqrt{E|E-E_a|_+}}{\left\{2\sqrt{E|E-E_a|_+}+(|E-E_a|_++E)\left[e^{\theta(E)}-\frac{1}{4}(1-e^{-\theta(E)})\right]\right\}}, \tag{8}$$

where

$$\theta(E)=\begin{cases}0, & E>E_a\\ \dfrac{2}{\hbar F}\sqrt{2m(E_a-E)^3}, & E\leqslant E_a,\end{cases}$$
$$|E-E_a|_+\equiv[(E-E_a)^2+\gamma_F]^{1/2},$$
$$\gamma_F\equiv(p_0^2\hbar^2F^2/2m)^{2/3}, \tag{9}$$

where in the notation following Ref. 38 F is the product of electric field and unit charge, and $p_0=0.516\,97$. Observe that $\exp[\theta(E)]>10^3$ for $E<E_a-(6.91\hbar^2F^2/2m)^{1/3}$. For typical fields, e.g., 1 MV/m, tunneling [that is, $D_\Delta(E<E_a)$] is significant only for $E_a-E<1/80$ eV, and therefore, the zero-field limit of Eq. (8) can be used in comparison to experimental data of Spicer and Taft and Philipp, for which

$$\lim_{F\to0}D_\Delta(E>E_a)=\frac{4\sqrt{E(E-E_a)}}{[\sqrt{(E-E_a)}+\sqrt{E}]^2}. \tag{10}$$

Representative cases are shown in Fig. 2, where energy is measured with respect to the bottom of the conduction band

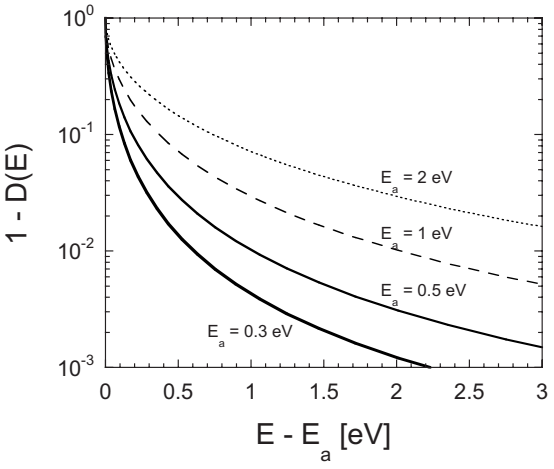

FIG. 2. Behavior of the transmission probability as a function of energy above the barrier maximum.

(rather than the top of the valence band). If, however, conditions were such that the field is 100 MV/m (for comparison, contemporary SRF guns use a gradient of 20 MV/m and future ones may use 50 MV/m,[4] and the on-axis field of the SPARC injector[39] and the FERMI *S*-band photoinjector[40] is 120 MV/m) then the range over which a tunneling current can contribute increases to 1/4 eV from the barrier maximum, comparable in size to, for example, the electron affinity of Cs_3Sb, and would necessitate the usage of Eq. (8) in Eq. (4).

Electron affinity

The approximation in the three-step model of Spicer that the transmission probability is a step function in energy rather than of the form of Eq. (10) has consequences in the choice of the electron affinity, as shown in Fig. 3. This can be seen most readily by considering Eq. (6). Let the electron affinity predicted from QE data under the step-function transmission probability approximation be designated E_a^* and that predicted using Eq. (10) be designated E_a. Then the equation for QE_0 indicates that the (numerical) solution of

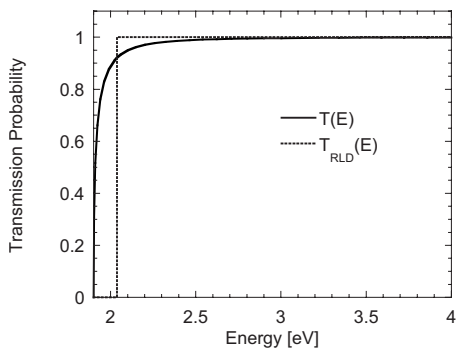

FIG. 3. Comparison of the transmission probability as a function of energy above the valence (not conduction) band: Energy so defined correlates with photon energy. The dashed line corresponds to Richardson approximation, in which the transmission probability is a step function $\Theta(E-E_a-E_g)$.

$$\int_{E_a}^{\Delta} ED_{\Delta}(E)F_{\lambda}\left(\sqrt{\frac{E}{E_a}}\right)dE = \int_{E_a^*}^{\Delta} EF_{\lambda}\left(\sqrt{\frac{E}{E_a}}\right)dE \qquad (11)$$

is the leading order approximation for E_a. We find if E_a^* =0.438 eV (the Table I Spicer value), then E_a=0.3033 eV; alternately, if E_a^*=0.276 eV (the Table I Taft and Philipp value), then E_a=0.1832 eV. In both evaluations using Eq. (11), the wavelength was taken to be 355 nm, corresponding to a photon energy of 3.493 eV. The results do not change much for other wavelengths.

Scattering

Relaxation time

Scattering principally affects the QE through the $p(E)$ factor in Eq. (4) most obviously not only in the presence of the relaxation time $\tau(E)$ but also in factors buried in the evaluation of the laser penetration depth $\delta(\hbar\omega)$ using models for the evaluation of the complex dielectric constant. Relaxation times for various mechanisms add inversely (Matthiessen's rule):[41,42] In the case of metals, the dominant contributions were acoustic and electron-electron scattering,[10,42] but for polar semiconductors, polar optical scattering and ionized impurity scattering are of greater importance[43–46] and so

$$\left.\frac{1}{\tau(E)}\right|_{\text{semi}} \approx \frac{1}{\tau_{\text{pop}}(E)} + \frac{1}{\tau_{ii}(E)} + \frac{1}{\tau_{\text{ac}}(E)}, \qquad (12)$$

where other scattering mechanisms typical of semiconductor transport[47] are generally much smaller, and where, for photon energies smaller than 4 eV, scattering of photoexcited electrons by valence electrons can be ignored.[21] In Eq. (12), E refers to the energy of the photoexcited electron as it begins its journey to the surface: Consequently, $\tau(E)$ is in contrast to the energy-averaged relaxation time $\langle\tau\rangle$ found in, for example, transport simulations and calculations of semiconductor mobility and dc conductivity (and which appears below in the Drude model).

The alpha-semiconductor model

Physical parameters required for the evaluation of Eq. (12) can be scarce for semiconductors of interest for photocathodes, motivating the reliance on a theoretical model in which these parameters can be approximated. A recently developed model of a generic or alpha-semiconductor[48] can provide what is required for present needs. Briefly, drawing analogies to the Bohr model of the hydrogen atom, the alpha-semiconductor model posits that the upper limit on electron velocity inside the semiconductor is limited to $\alpha_{\text{fs}}c/2$, where α_{fs} is the fine structure constant, and sets the band gap equal to $E_g=\alpha_{\text{fs}}^2 mc^2/2$. The latter relation entails that the effective mass of the electron is related to the band gap via

$$\frac{m}{m_0} = \frac{E_g}{R_\infty}, \qquad (13)$$

where R_∞ is the Rydberg energy 13.606 eV. The alpha-semiconductor model provides a large simplification in the calculation of a material's optical constants, though the concern here is with its relation to the calculation of scattering

terms and the relationship for the effective mass to the band gap. In particular, the polar optical and ionized impurity scattering rates will be calculated as though they are alpha-semiconductors. We parenthetically note that the related materials CdTe and AlSb are well characterized by the alpha-semiconductor model and they have band gaps close to Cs_3Sb.

Acoustic phonon

Acoustic phonon scattering is calculated according to the analogous expression found for metals[10] as follows:

$$\frac{1}{\tau_{\rm ac}} = \frac{4mk_BT_D\Xi^2}{\pi\hbar^3\rho\nu_s^2}\left(\frac{2mE}{\hbar^2}\right)^{1/2}\left(\frac{T}{T_D}\right)^6 W_-\left(5,\frac{T_D}{T}\right), \tag{14}$$

where $W_-(5,x)$ is the Bloch–Grüneisen function (approximate by $x^4/4$ for small x), T_D is the Debye temperature, Ξ is the deformation potential, ν_s is the sound velocity, and ρ is the mass density. For small Debye temperatures, $1/\tau_{\rm ac}$ is approximately linear in temperature: The resulting form is the quasiclassical limit of the quantum mechanical expression[44] and corresponds to the Bardeen–Shockley result.[49] We find that compared to polar optical, acoustic is negligible, a not unexpected result.

Polar optical phonon

The expression from polar optical phonon scattering can be obtained from Eq. (56) and Appendix C of Ref. 44. In the usual parabolic band approximation with the assumption that the Kane overlap wave-function factor is unity, the standard result is

$$\begin{aligned}\frac{1}{\tau_{\rm pop}(\hbar\omega_q,E)} &\approx \frac{q^2\omega_q}{2\pi\varepsilon_0\hbar\nu_k}\left(\frac{1}{K_\infty}-\frac{1}{K_0}\right)n(\hbar\omega_q)\\ &= \frac{2\alpha_{\rm fs}\omega_q c}{\nu_k}\Delta\varepsilon n(\hbar\omega_q),\\ \Delta\varepsilon &= \left(\frac{1}{K_\infty}-\frac{1}{K_0}\right),\end{aligned} \tag{15}$$

where $E_k \equiv E = m\nu_k^2/2$ relates the electron velocity to its energy, and K_∞ and K_0 are the high frequency and static dielectric constants (corresponding to ε_∞ and ε_0 in cgs units) such that $\Delta\varepsilon$ is generally on the order of 10^{-2}. Equation (15) compares, for example, to the $\hbar\omega_q \ll E$ and $n(\hbar\omega_q) \gg 1$ limit of the expression for polar optical scattering in conventional treatments.[41,47] In a quantum mechanical treatment using the alpha-semiconductor model, however, $1/\tau_{\rm pop}$ is the sum of the emission and absorption rates defined by

$$\begin{aligned}\frac{1}{\tau_\pm(\hbar\omega_q,E)} &= 4\omega_q\Delta\varepsilon\left(n(\hbar\omega_q)+\frac{(1\mp 1)}{2}\right)\\ &\times\left[\frac{\gamma(u_\pm)^2}{\beta(u_\pm)}d(u,u_\pm)\right],\end{aligned} \tag{16}$$

where $u_\pm \equiv u \pm y \equiv (E \pm \hbar\omega_q)/E_g$ (the k subscript on E is suppressed) and where the choice of sign designates emission or absorption of a phonon of energy $\hbar\omega_q$. The functions $\gamma(u)$ and $\beta(u)$ are defined by

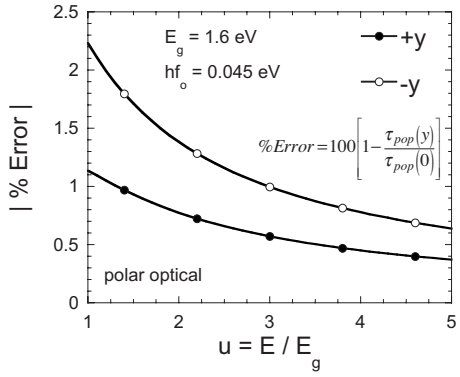

FIG. 4. Error in the inverse polar optical relaxation time as a consequence of neglecting higher order terms in phonon energy.

$$\gamma(u) = \frac{1}{\sqrt{1-\beta(u)^2}} = 1+2u \tag{17}$$

and the Bose–Einstein distribution n is defined by

$$n(\hbar\omega_q) = \frac{1}{\exp\left(\frac{\hbar\omega_q}{k_BT}\right)-1}. \tag{18}$$

The polar optical scattering rate is then given by

$$\frac{1}{\tau_{\rm pop}} = \frac{1}{\tau_+}+\frac{1}{\tau_-}. \tag{19}$$

The function $d(u,u_\pm)$ is treated at length in Refs. 44 and 48 and its complexity frustrates a compact representation. It may be considerably simplified in the limit that $\hbar\omega_q \ll E$, for which to leading order in y

$$d(u,u\pm y) \approx \frac{16u^2+18u+3}{3(1+2u)^4} \pm y\ln(2)\frac{2u^2+2u+1}{(1+2u)^5}. \tag{20}$$

Recall that y is the ratio between phonon energy and the band gap: For Cs_3Sb, the electron energies of interest will be in excess of the electron affinity (0.45 eV) whereas the phonon energy for polar semiconductors is generally less than 0.05 eV: Under such circumstances, the $y=0$ limit of Eq. (16) is of reasonable accuracy (better than 4%) for numerical evaluations. The $y=0$ (leading order) approximation for $d(u,u)$ is

$$\frac{1}{\tau_{\rm pop}(\hbar\omega_q,E)} \approx 2\omega_q\Delta\varepsilon[2n(\hbar\omega_q)+1]\frac{16u^2+18u+3}{3(1+2u)\sqrt{u(u+1)}}. \tag{21}$$

The percentage difference between $(1/\tau_{\rm pop})$ and its $y=0$ approximation (i.e., $u_\pm \to u$) is shown in Fig. 4 for representative values. Clearly, for electron energies comparable to the band gap, the departure between Eqs. (21) and (15) is noticeable. Additionally, for $u \gg 1$, Eq. (21) approaches $(16/3)\omega_q\Delta\varepsilon[2n(\hbar\omega_q)+1]$. For the energy range of present interest, however, Eq. (21) is good.

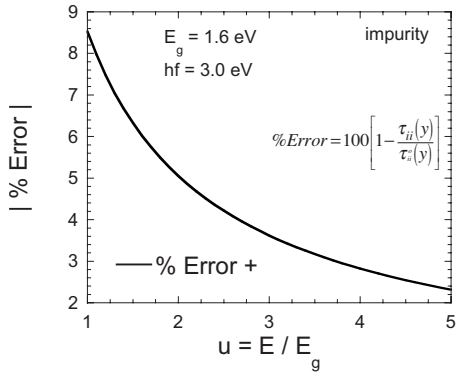

FIG. 5. Same as Fig. 4, but for the impurity scattering relaxation time.

Ionized impurity

The relaxation time for impurity scattering in the alpha-semiconductor model is given by[48]

$$\frac{1}{\tau^I(E)} = \frac{8\pi\hbar^2}{\alpha_{\rm fs} m^2 c}\left(\frac{N_i}{K_0^2}\right)\left[\frac{\gamma^2(u+y)}{4\beta(u+y)} d^I(u,u+y)\right], \tag{22}$$

where N_i is the impurity concentration (number density) of the impurities, and (as before) $u=E/E_g$, $y=\hbar\omega_q/E_g$, and where [analogous to Eq. (20)] for numerical work, only the leading order term for $d^I(u,u+y)$ need be retained, for which

$$\frac{1}{\tau^I(E)} \approx \frac{8\pi\hbar^2}{\alpha_{\rm fs} m^2 c}\left(\frac{N_i}{K_0^2}\right)\left[\frac{\ln(2)}{\beta(u)\gamma(u)}\right]\left(\frac{1}{y}\right)$$
$$= \frac{4\pi\hbar^2}{\alpha_{\rm fs} m^2 c}\left(\frac{N_i}{K_0^2}\right)\ln(2)\left(\frac{E_g^2}{\hbar\omega\sqrt{E(E+E_g)}}\right). \tag{23}$$

The coefficient is familiar from the Brooks–Herring model,[50] but the energy dependence is not similar as a consequence of the energy regime leading to Eq. (23). As has been found in the case of InP and GaAs,[51] impurity scattering even for relatively high concentrations (e.g., $N_i=10^{17}$ #/cm^3) does not appear to contribute significantly for high photon energies and temperatures, but it is nevertheless included for completeness and because the character of Cs_3Sb is changed when an excess of cesium is present.[31] The percentage difference between $(1/\tau^I)$ calculated exactly in Eq. (22) and its approximation by Eq. (23) is shown in Fig. 5 for representative values and a typical photon energy of 3 eV. Though the error can be up to 8% for the range chosen, we find below that (as anticipated) the contribution of τ_{ii} is small compared to polar optical, and therefore the impact of the error is negligible.

Reflection and penetration

The estimation of the optical constants shall be made using a combination of experimental data and a variation on the Drude–Lorentz model for the complex dielectric constant.[42,45] While spline-fitting actual data may seem preferable, as has been done before in the case of metals,[7,8,10] the optical data are scant for Cs_3Sb for higher photon energy needed herein, and splining what is available is counter to the needs of a theoretical model.

The dielectric constant (in MKSA units) may be written as

$$\varepsilon = \varepsilon_0(n-ik)^2, \tag{24}$$

where n is the index of refraction and k is the extinction coefficient. The Drude model then relates n and k to the zero and high frequency dielectric constants (K_0 and K_∞) and the plasma frequency

$$\omega_p^2 = \frac{q^2\rho_e}{\varepsilon_0 m} = 4\pi\rho_e\frac{\alpha_{\rm fs}\hbar c}{m} \tag{25}$$

by the relations

$$n^2 - k^2 = K_\infty - \frac{(\omega_p\tau)^2}{(\omega\tau)^2+1},$$
$$2nk = \frac{\tau\omega_p^2}{\omega[(\omega\tau)^2+1]}. \tag{26}$$

These equations can be obtained by considering a model of a bound electron treated as a harmonic oscillator in an electric field with a dampening term given by (m/τ) in which the restoring force given by $m\omega_0^2$ is weak [e.g., Eq. (403) of Ref. 42]. If the restoring force is not neglected, however, then, in a form modified from that given by Sanderson[52] (see also Ref. 53)

$$n^2 - k^2 \Rightarrow K_\infty + (K_0 - K_\infty)\frac{\omega_T^2(\omega_T^2-\omega^2)}{(\omega^2-\omega_T^2)^2+(\gamma_0\omega_T\omega)^2} - \frac{(\omega_p\tau)^2}{1+(\omega\tau)^2},$$
$$2nk \Rightarrow (K_0 - K_\infty)\frac{\gamma_0\omega\omega_T^3}{(\omega^2-\omega_T^2)^2+(\gamma_0\omega_T\omega)^2} - \frac{\tau\omega_p^2}{\omega[1+(\omega\tau)^2]}, \tag{27}$$

where ω_T is the transverse optical mode, γ_0 is a dimensionless constant, ω_p is the plasma frequency, and the terms containing it are from the Drude model, for which the term τ is an energy-averaged summation over the various scattering components. On the assumption that the number of free carriers in the conduction band is not large, the Drude terms in Eq. (27) are negligible as ω_p is negligible. For available optical n and k data, the parameters γ_0, ω_T, K_s, and K_∞ can be determined, from which the reflectivity R and penetration depth δ are evaluated via

$$R = \frac{(n-1)^2+k^2}{(n+1)^2+k^2}, \quad \delta = \frac{c}{2k\omega} = \frac{\lambda}{4\pi k}. \tag{28}$$

Optical constants are subject to some variation: As a typical example, consider the variation evinced in a set of four bialkali cathodes as studied by Harmer *et al.*[54] As shown in Fig. 6, the variation (average, maximum, and minimum values) for three S20 photocathode samples reported in Table 1 of Harmer *et al.* shows generally consistent trends but nevertheless a range of values that were attributed to variations in the cathode material during the formation stage, thereby leading to variations in the optical properties. In particular, the difference between the reflection factor R calculated using the maximum or minimum values of n and k in Fig. 6 is shown in Fig. 7. In a like manner, variation in optical data for Cs_3Sb should be anticipated (and is, in fact, observed[55]).

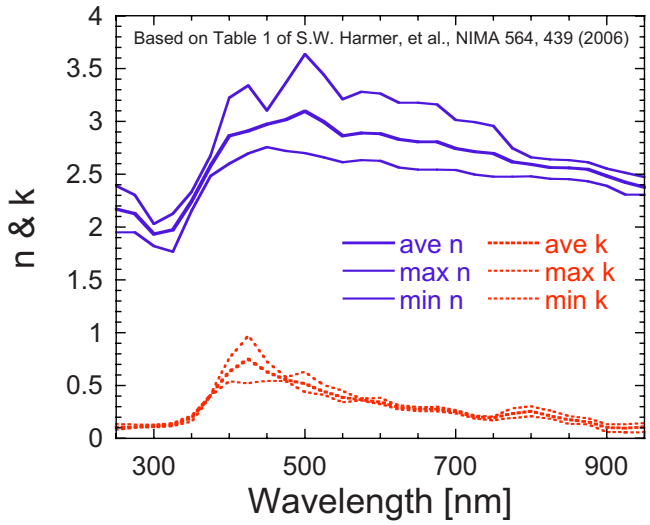

FIG. 6. (Color online) Maximum and minimum optical parameters n and k for a related multialkali material, showing variation; the solid middle line is the average of all three measurements.

Thus, though the values of γ_0, ω_T, K_s, and K_∞ shall be based on the single parameter set (n,k) deduced for the limited wavelength range 400 nm$<\lambda<$1.8 nm (shown in Fig. 6 of Wallis in Ref. 56), it is to be expected that variations in R comparable to Fig. 7 should exist.

The values of γ_0, ω_T, and (K_0-K_∞) were determined from $2nk$, and the value of K_∞ from n^2-k^2, as shown in Fig. 8; the values settled upon are listed in Table II. The resulting calculation of the reflectivity of Cs_3Sb is shown in Fig. 9, along with the reflectivity of a multialkali material as measured by Ghosh[57] for comparison: The differences make plausible the notion that using one-Lorentzian term in Eq. (27) is likely inadequate, a conjecture reinforced by considering the related material InSb for which the optical properties are well studied.[58] A one-Lorentzian model is shown to be lacking at higher energies, as shown in Fig. 10, for InSb, and a similar deficiency may explain the high energy departures between theory and experiment below.

SIMULATION OF THE QE OF CS_3SB AND DISCUSSION

Several parameters listed in Table II are determined via various sources and models. The Debye temperature was taken as the larger value of the two quoted values of 59 K for

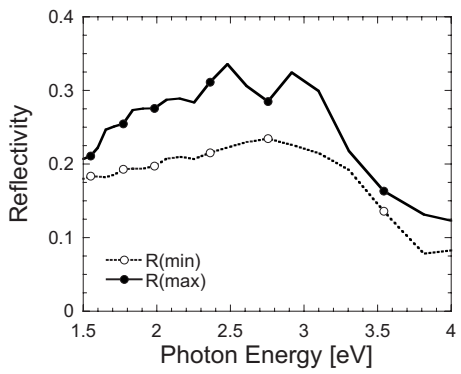

FIG. 7. Reflectivity as calculated using the maximum and minimum n and k values shown in Fig. 4.

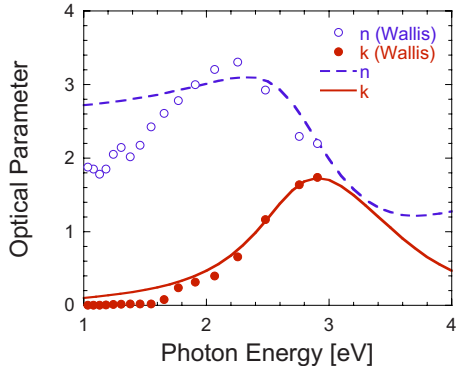

FIG. 8. (Color online) The optical n and k parameters for Cs_3Sb and their approximation based on the Lorentz model.

Cs and 131 K for Sb in Cs_3Sb.[59] This factor figures in the acoustic phonon relaxation time and is therefore not of significant impact. The band gap and electron affinity of Cs_3Sb are well known.[14,31,60] The impurity concentration was taken to be representative of low concentration values (not "pure") typical of III-V and II-VI semiconductors.[44] The sound velocity was inferred from the elastic constant c_{11} and the mass density ρ by the relation $\nu_s=\sqrt{c_{11}/\rho}$. Choosing ρ to be the ratio of the mass of atoms in a unit cell (which contains four Cs_3Sb) with the unit cell volume L^3 of Cs_3Sb, where $L=0.9128$ nm,[61] that is, $\rho=4(3M_{Cs}+M_{Sb})/L^3=4.5191$ g/cm^3 for $M_{Cs}=132.91$ g/mole and $M_{Sb}=118.71$ g/mole (a value comparing favorably to the microscopic density quoted by Imamua[62]) and $L=0.9128$ nm, and letting c_{11} be a "generic" semiconductor value of 12×10^{12} N/m^2 (as inferred from various sources[49,53]) suggests $\nu_s\approx5153$ m/s. The phonon energy $\hbar\omega_q$ is crudely related to the sound velocity in the relation suggested by Ridley[63] of $\hbar\omega_q\approx4\pi\hbar\nu_s/L\approx0.05$ eV, a value comparable to (but slightly larger than) other semiconductors.[45] As Ridley noted, the deformation potential energy is difficult to ascertain, but using his "guess" of the mean deformation potential constant $D=5\times10^8$ eV/cm and letting l be comparable to the average of the ionic radii of Cs and Sb gives $\Xi\approx Dl\approx7$ eV. Note that sound velocity and deformation potential appear in ratio in the acoustic phonon scattering rate, which is a minor player in the evaluation of τ. All other parameters are determined via the alpha-semiconductor model and other models introduced above.

The Cs_3Sb data to be simulated have been extracted from Fig. 8 of Spicer[14] and shown also in Fig. 11, where QE_0 is given in Eq. (6) and $QE_{total}=QE_0+\Delta QE$ refer to the moments-based approach and correction factor. Apart from the behavior near 4 eV (likely traceable to aforementioned deficiencies related to the Lorentz model to obtain reflectivity and penetration depth), the agreement is good especially considering that *all* of the parameters for the theoretical model are based on fundamental models and values extracted from literature—in other words, no fitting or parametrization was performed as there are no parameters to vary. An alternate representation of Fig. 11 is given in Fig. 12 and based on the empirical relation suggested by Eq. (1) for the 300 K data and the simulation results (but note that Spicer took $E_a=0.45$ eV whereas Fig. 12 uses $E_a+E_g=E_0=2.038$ eV).

The quality of the simpler model of QE given by Eq. (6)

TABLE II. Parameters and defining or representative values used in simulation for Cs_3Sb.

Parameter	Symbol	Unit	Value
Electron rest mass	m_0	eV/c^2	0.056 86
Band gap	E_g	eV	1.6
Electron affinity[a]	E_a	eV	0.303 3 (s) 0.183 2 (t)
Static dielectric constant	K_0	⋯	5.0
High frequency dielectric constant	K_∞	⋯	8.2
Impurity concentration	N_i	$\#/cm^3$	10^{17}
Photon energy	$\hbar\omega$	eV	≤4
Phonon energy	$\hbar\omega_q$	eV	0.05
Sound velocity	v_s	m/s	5153
Deformation potential	Ξ	eV	7
Debye temperature	T_D	K	131
Rydberg energy	R_∞	eV	13.606
Laser intensity	I_0	MW/cm^2	1
Applied field	F/q	MV/m	1
Mass density	ρ	g/cm^3	4.519
Fine structure constant	$\alpha_{fs}=q^2/4\pi\varepsilon_0\hbar\omega$	⋯	1/137.036
Transverse optical phonon	ω_T	10^{15} rad/s	4.22
Lorentz coefficient	γ_0	⋯	0.375
Effective mass	$(E_g/R_\infty)m_0$	eV/cm^2	

[a]The electron affinity used to compare with the data of Spicer is labeled with (s) and that to compare with the data of Taft and Philipp is labeled with (t).

is assessed and presented in Fig. 13. Not surprisingly, at low values of $\hbar\omega - E_g - E_a$, the QE_0 model is progressively worse as the range of energies of the photoemitted electrons becomes increasingly constrained and the behavior of the transmission probability near the barrier maximum becomes more consequential. However, it is also clear that QE_0 functions quite well as a first pass estimation of the QE of a semiconductor.

Finally, using the different value of E_a suggested by Taft and Philipp, a comparison to their data is made. All parameters apart from electron affinity were held the same as Spicer's and are given in Table II. Apart from a scale factor of 1.4, again, the agreement is satisfactory.

In the absence of adjustable parameters, such agreement is notable, but discussion of sources of discrepancies is nevertheless required.

- The reflectivity and penetration depth were based on a simple (Lorentz) model of the optical constants, but the behavior of the constants for photon energies in excess of 3.1 eV (corresponding to a wavelength of 400 nm) was not available. Nevertheless, the mean free paths calculated herein are commensurate with estimates and calculations elsewhere.[31,64] However, the reflectivity calculated via the analytical model tended to be smaller than some measurements reported in literature at longer wavelengths, thereby causing the theoretical model to be slightly reduced in QE by comparison.
- Eckart[27] argued that the band gap lay between 1.6 and 1.9 eV whereas the lower value suggested by Spicer was used uniformly in simulation.
- The alpha-semiconductor parameters were instrumental in obtaining the theoretical model, but it is not clear

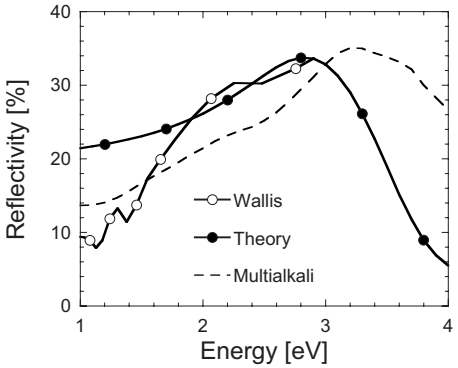

FIG. 9. Reflectivity as measured by Wallis (Ref. 56) compared to the Lorentz model. Also shown is the reflectivity of a multialkali photocathode for comparison from Ref. 57.

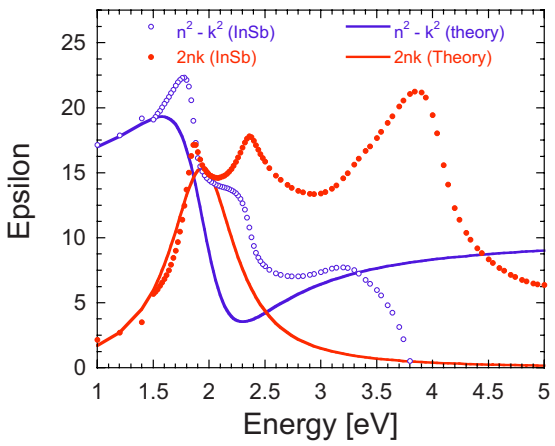

FIG. 10. (Color online) Real and imaginary parts of the dielectric constant for InSb and its approximation using a one-component Lorentz model: The need for several Lorentz components is indicated by the failure of the one-component model to capture behavior at higher energies.

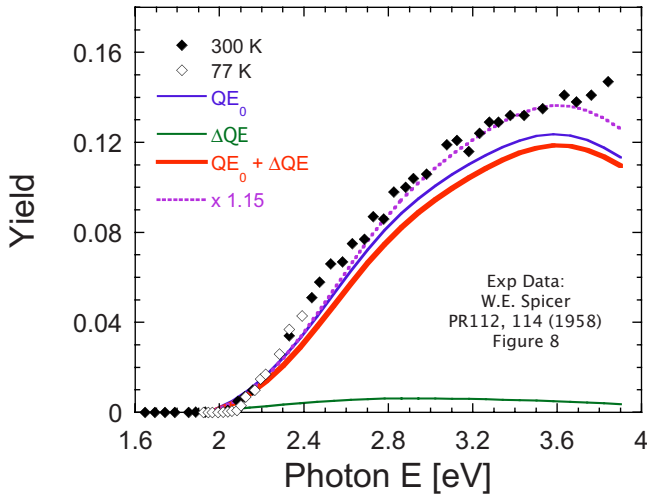

FIG. 11. (Color online) Comparison of the experimental measurement of QE from Spicer compared to the simulations based on the theoretical models developed herein using the values listed in Table II. No adjustable parameters were used. The theory multiplied by a scale factor of 1.15 brings the simulation into good agreement.

how well Cs_3Sb is modeled by an alpha-semiconductor, even though a number of similar semiconductors satisfy the criteria well. For example, CdTe is the best alpha-semiconductor[48] and has a band gap of 1.5 eV, close to Cs_3Sb.

- A slight excess of Sb renders Cs_3Sb *p*-type whereas excess Cs acts as donors,[16,65] and Cs_3Sb can therefore be made *n*-type:[31] This may account for some differences reported for the experimental measurements, but does not (as yet) have a theoretical model to account for the impact on the band bending.
- Electron-electron scattering, known to be very important for affecting the yield, has not been included because its threshold occurs at a photon energy greater than 4 eV.[21] Ionized impurity and acoustic phonon scattering effects are small and negligible, respectively, for present parameters, though this was not *a priori* so.

CONCLUSION

A model of photoemission is given that does not rely on the usage of adjustable parameters to obtain correspondence

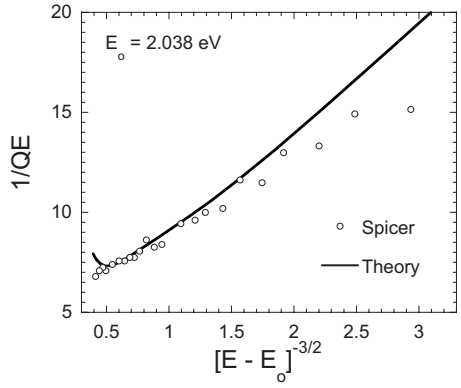

FIG. 12. Same as Fig. 9, but using the energy coordinates suggested by the three-step model of Spicer.

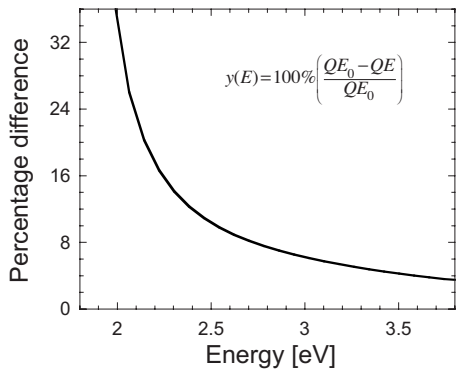

FIG. 13. Percentage difference between the full multidimensional moments-based QE integral with the simpler one-dimensional approximation based on neglecting the polar angle term in the transmission probability.

with experimental data on the QE of cesium antimonide (Cs_3Sb). The model made use of a moments-based approach to calculate QE with the following components. First, an analytical transmission probability for a triangular-barrier potential was used. Second, the evaluation of the relaxation time (scattering rates) made use of a theoretical model of an "alpha-semiconductor" to obtain parameters. Three scattering mechanisms were considered, namely, acoustic phonon, polar optical phonon, and impurity scattering, the last two being defined in the context of the alpha-semiconductor model, of which the polar optical contribution dominates. Finally, an analytical Lorentz model was used to infer reflectivity and penetration depth. All parameters were extracted from literature without regard to their impact on the estimation of QE. The agreement between the experimental data of Spicer and Taft and Philipp remained quite good up to factors of 15% and 40%, respectively. Factors that may affect the comparison were discussed.

As a final observation, it is noted that the evaluation of QE requires the full multidimensional moments-based approach of Eq. (3), which requires numerical integration over

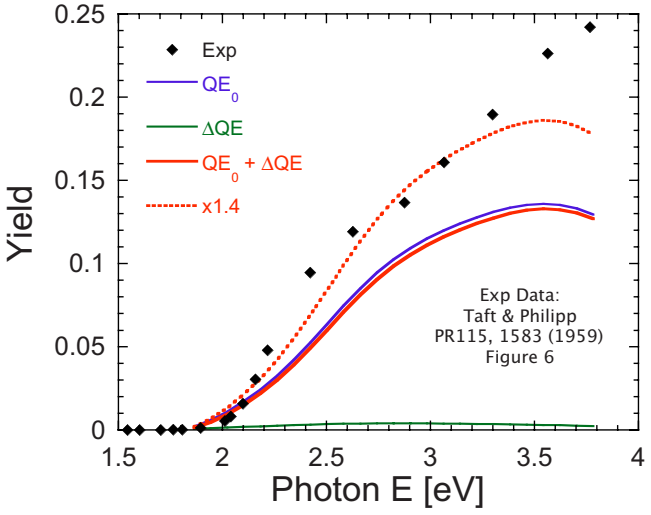

FIG. 14. (Color online) Comparison of the experimental measurement of QE from Taft and Philipp compared to the simulations based on the theoretical models developed herein using the values listed in Table II. No adjustable parameters were used. The theory multiplied by a scale factor of 1.4 brings the simulation into good agreement.

two dimensions. A simpler one-dimensional model obtained by ignoring the dependence of the transmission probability on the polar angle allows for a much easier numerical integration of an analytical function based on Eq. (6) and, to within 10%–20% accuracy for photon energies of interest, has proven useful for more numerically tractable estimations of QE as would be needed by, for example, beam simulartion codes under development.[13]

ACKNOWLEDGMENTS

We thank the Joint Technology Office and the Office of Naval Research for supporting this work.

[1]N. A. Moody, K. L. Jensen, D. W. Feldman, E. J. Montgomery, and P. G. O'Shea, J. Appl. Phys. **102**, 104901 (2007).
[2]P. Michelato, Nucl. Instrum. Methods Phys. Res. A **393**, 455 (1997).
[3]S. H. Kong, J. Kinross-Wright, D. C. Nguyen, and R. L. Sheffield, Nucl. Instrum. Methods Phys. Res. A **358**, 272 (1995).
[4]C. Hernandez-Garcia, P. G. O'Shea, and M. L. Stutzman, Phys. Today **61**(2), 44 (2008).
[5]E. J. Montgomery, D. W. Feldman, P. G. O'Shea, Z. Pan, N. Sennett, K. L. Jensen, and N. A. Moody, J. Directed Energy (submitted).
[6]C. Travier, Nucl. Instrum. Methods Phys. Res. A **304**, 285 (1991).
[7]K. L. Jensen, D. W. Feldman, M. Virgo, and P. G. O'Shea, Phys. Rev. ST Accel. Beams **6**, 083501 (2003).
[8]K. L. Jensen, D. W. Feldman, N. A. Moody, and P. G. O'Shea, J. Appl. Phys. **99**, 124905 (2006).
[9]N. A. Moody, K. L. Jensen, D. W. Feldman, P. G. O'Shea, and E. J. Montgomery, Appl. Phys. Lett. **90**, 114108 (2007).
[10]K. L. Jensen, N. A. Moody, D. W. Feldman, E. J. Montgomery, and P. G. O'Shea, J. Appl. Phys. **102**, 074902 (2007).
[11]D. A. Dimitrov, D. L. Bruhwiler, J. R. Cary, P. Messmer, P. Stoltz, K. L. Jensen, D. W. Feldman, and P. G. O'Shea, "Development of Advanced Models for 3D Photocathode PIC simulations," Proceedings of the Particle Accelerator Conference, 2005, pp. 2583–2585, 16–20 May 2005.
[12]J. J. Petillo, E. M. Nelson, J. F. Deford, N. J. Dionne, and B. Levush, IEEE Trans. Electron Devices **52**, 742 (2005).
[13]K. L. Jensen, J. J. Petillo, E. J. Montgomery, Z. Pan, D. W. Feldman, P. G. O'Shea, N. A. Moody, M. Cahay, J. E. Yater, and J. L. Shaw, J. Vac. Sci. Technol. B **26**(2), 831 (2008).
[14]W. E. Spicer, Phys. Rev. **112**, 114 (1958).
[15]C. N. Berglund and W. E. Spicer, Phys. Rev. **136**, A1030 (1964).
[16]A. H. Sommer and W. E. Spicer, in *Photoelectronic Materials and Devices*, edited by S. Larach (Van Nostrand, Princeton, NJ, 1965), p. 175.
[17]W. E. Spicer, J. Vac. Sci. Technol. A **3**, 461 (1985).
[18]W. E. Spicer and A. Herrera-Gomez, Proc. SPIE **2022**(1), 18 (1993).
[19]D. H. Dowell, F. K. King, R. E. Kirby, J. F. Schmerge, and J. M. Smedley, Phys. Rev. ST Accel. Beams **9**, 063502 (2006).
[20]E. O. Kane, Phys. Rev. **127**, 131 (1962).
[21]L. Apker, E. Taft, and J. Dickey, J. Opt. Soc. Am. **43**, 78 (1953).
[22]A. H. Sommer, J. Appl. Phys. **29**, 1568 (1958).
[23]K. L. Jensen, P. G. O'Shea, D. W. Feldman, and N. A. Moody, Appl. Phys. Lett. **89**, 224103 (2006).
[24]F. Wooten and W. E. Spicer, Surf. Sci. **1**, 367 (1964).
[25]F. Wooten, J. P. Hernandez, and W. E. Spicer, J. Appl. Phys. **44**, 1112 (1973).
[26]E. A. Taft and H. R. Philipp, Phys. Rev. **115**, 1583 (1959).
[27]F. Eckart, Ann. Phys. **19**, 133 (1956).
[28]N. V. Smith and G. B. Fisher, Phys. Rev. B **3**, 3662 (1971).
[29]U. Muller, H. Burtscher, and A. Schmidtott, Phys. Rev. B **38**, 7814 (1988).
[30]A. Herrera-Gomez and W. E. Spicer, SLAC-PUB-6307 (1993).
[31]A. Natarajan, A. T. Kalghatgi, B. M. Bhat, and M. Satyam, J. Appl. Phys. **90**, 6434 (2001).
[32]J. Smedley, T. Rao, and J. Sekutowicz, Phys. Rev. ST Accel. Beams **11**, 013502 (2008).
[33]B. Erjavec, Thin Solid Films **303**, 4 (1997).
[34]A. Modinos, *Field, Thermionic, and Secondary Electron Emission Spectroscopy* (Plenum, New York, 1984).
[35]R. H. Fowler, Phys. Rev. **38**, 45 (1931).
[36]K. L. Jensen, J. Vac. Sci. Technol. B **21**, 1528 (2003).
[37]R. H. Fowler and L. Nordheim, Proc. R. Soc. London, Ser. A **119**, 173 (1928).
[38]K. L. Jensen, J. Appl. Phys. **102**, 024911 (2007).
[39]J. Rosenzweig, A. Cook, R. England, M. Dunning, S. Anderson, and M. Ferrario, Nucl. Instrum. Methods Phys. Res. A **557**, 87 (2006).
[40]G. D'Auria, D. Bacescu, L. Badano, F. Cianciosi, P. Craievich, M. Danailov, G. Penco, L. Rumiz, M. Trovo, A. Turchet, H. Badakov, A. Fukusawa, B. O'Shea, and J. B. Rosenzweig, "The new photoinjector for the FERMI project," Particle Accelerator Conference, 2007, pp. 974–976, 25–29 June 2007.
[41]M. Lundstrom, *Fundamentals of Carrier Transport* (Cambridge University Press, Cambridge, UK, 2000).
[42]K. L. Jensen, *Advances in Imaging and Electron Physics*, Electron Emission Physics Vol. 149 (Academic, New York, 2007).
[43]B. Jensen, Ann. Phys. (N.Y.) **95**, 229 (1975).
[44]B. Jensen, in *Reviews of Infrared and Millimeter Waves*, edited by K. J. Button (Academic, New York, 1983), Vol. 8, p. 127.
[45]B. Jensen, in *Handbook of Optical Constants of Solids*, edited by E. D. Palik (Academic, Orlando, FL, 1985), p. 169.
[46]B. Jensen, in *Handbook of Optical Constants of Solids II*, edited by E. D. Palik (Academic, Boston, MA, 1991), p. 125.
[47]B. K. Ridley, *Quantum Processes in Semiconductors* (Clarendon, Oxford, 1999).
[48]B. L. Jensen and K. L. Jensen, Ann. Phys. (submitted).
[49]J. Bardeen and W. Shockley, Phys. Rev. **80**, 72 (1950).
[50]B. K. Ridley, J. Phys. C **10**, 1589 (1977).
[51]B. Jensen, Ann. Phys. (N.Y.) **80**, 284 (1973).
[52]R. B. Sanderson, J. Phys. Chem. Solids **26**, 803 (1965).
[53]H. Ibach and H. Lüth, *An Introduction to Principles of Materials Science* (Springer, Berlin, 2003).
[54]S. W. Harmer, R. Downey, Y. Wang, and P. D. Townsend, Nucl. Instrum. Methods Phys. Res. A **564**, 439 (2006).
[55]G. Wlérick and A. Grosse, in *Advances in Electronics and Electron Physics*, edited by J. D. McGee, D. McMullan, and E. Kahan (Academic, London, 1966), Vol. 22A.
[56]G. Wallis, Ann. Phys. **452**, 401 (1956).
[57]C. Ghosh, Phys. Rev. B **22**, 1972 (1980).
[58]R. T. Holm, in *Handbook of Optical Constants of Solids*, edited by E. D. Palik (Academic, Orlando, 1985), p. 491.
[59]K. H. Jack and M. M. Wachtel, Proc. R. Soc. London, Ser. A **239**, 46 (1957).
[60]W. E. Spicer, J. Appl. Phys. **31**, 2077 (1960).
[61]L. I. Berger, in *CRC Handbook of Chemistry and Physics*, 88th ed., edited by D. R. Lide (CRC, Boca Raton, FL, 2007), p. 12.141.
[62]S. Imamura, J. Phys. Soc. Jpn. **14**, 1491 (1959).
[63]B. Ridley, J. Appl. Phys. **48**, 754 (1977).
[64]W. E. Spicer, J. Phys. Chem. Solids **22**, 365 (1961).
[65]M. Berndt and P. Görlich, Phys. Status Solidi **3**, 963 (1963).